ORIGINAL ARTICLE

Transcription factor EHF interacting with coactivator AJUBA aggravates malignancy and acts as a therapeutic target for gastroesophageal adenocarcinoma

Li Peng[a,b], Yanyi Jiang[c], Hengxing Chen[a], Yongqiang Wang[a,b],
Qiusheng Lan[d], Shuiqin Chen[a,b], Zhanwang Huang[a,b],
Jingyuan Zhang[a,b], Duanqing Tian[a,b], Yuntan Qiu[a], Diankui Cai[e],
Jiangyun Peng[a], Daning Lu[a,b], Xiaoqing Yuan[a,b,*], Xianzhu Yang[f,*],
Dong Yin[a,b,*]

[a]Guangdong Provincial Key Laboratory of Malignant Tumor Epigenetics and Gene Regulation, Guangdong-Hong Kong Joint Laboratory for RNA Medicine, Sun Yat-sen Memorial Hospital, Sun Yat-sen University, Guangzhou 510120, China
[b]Medical Research Center, Sun Yat-sen Memorial Hospital, Sun Yat-sen University, Guangzhou 510120, China
[c]Hefei Institutes of Physical Science, Chinese Academy of Sciences, Hefei 230031, China
[d]Department of Gastrointestinal Surgery, Sun Yat-sen Memorial Hospital, Sun Yat-sen University, Guangzhou 510120, China
[e]Department of Hepatobiliary Surgery, Sun Yat-sen Memorial Hospital, Sun Yat-sen University, Guangzhou 510120, China
[f]School of Biomedical Sciences and Engineering, South China University of Technology, Guangzhou International Campus, Guangzhou 511442, China

Abstract   Transcriptional dysregulation of genes is a hallmark of tumors and can serve as targets for cancer drug development. However, it is extremely challenging to develop small-molecule inhibitors to target abnormally expressed transcription factors (TFs) except for the nuclear receptor family of TFs. Little is known about the interaction between TFs and transcription cofactors in gastroesophageal adenocarcinoma (GEA) or the therapeutic effects of targeting TF and transcription cofactor complexes.

*Corresponding authors.

E-mail addresses: yuanxq7@mail.sysu.edu.cn (Xiaoqing Yuan), yangxz@scut.edu.cn (Xianzhu Yang), yind3@mail.sysu.edu.cn (Dong Yin).

In this study, we found that ETS homologous factor (EHF) expression is promoted by a core transcriptional regulatory circuitry (CRC), specifically ELF3-KLF5-GATA6, and interference with its expression suppressed the malignant biological behavior of GEA cells. Importantly, we identified Ajuba LIM protein (AJUBA) as a new coactivator of EHF that cooperatively orchestrates transcriptional network activity in GEA. Furthermore, we identified KRAS signaling as a common pathway downstream of EHF and AJUBA. Applicably, dual targeting of EHF and AJUBA by lipid nanoparticles cooperatively attenuated the malignant biological behaviors of GEA *in vitro* and *in vivo*. In conclusion, EHF is upregulated by the CRC and promotes GEA malignancy by interacting with AJUBA through the KRAS pathway. Targeting of both EHF and its coactivator AJUBA through lipid nanoparticles is a novel potential therapeutic strategy.

Enhancer;
Core transcriptional regulatory circuitry;
Gastroesophageal adenocarcinoma;
Gastric adenocarcinoma;
Esophageal adenocarcinoma;
Transcription factor;
Coactivator;
Lipid nanoparticles

1. Introduction

With 1,089,103 new cases in 2020, gastric cancer is the sixth most diagnosed general cancer worldwide[1]. Additionally, it accounted for 768,793 deaths, making it the third leading cause of cancer-related death according to Global Cancer Statistics 2020[1]. The high mortality rate can often be attributed to the diagnosis of gastric cancer in an advanced stage[2]. Gastric adenocarcinoma (GAC) is the most common histologic type, accounting for ~95% of primary gastric cancers[3]. Through a pooled analysis of mRNA expression, DNA methylation and somatic copy number analysis (SCNA) data, esophageal adenocarcinoma (EAC) has been found to have a profound similarity to gastric adenocarcinoma[4]. This finding suggests that GAC and EAC may be considered a single disease called gastroesophageal adenocarcinoma (GEA)[4]. Moreover, therapeutic strategies with proven efficacy in treating GEA[5] and numerous clinical trials (such as the JACOB trial[6], RAMSES/FLOT7 trial[7] and phase 3 JACCRO GC-07 trial[8]) for GEA all provided evidence that EAC and GAC comprise one disease. Despite great advances in science and the myriad of clinical trials over the past decade, minimal improvements in GEA patient outcomes have been achieved through improved therapeutic strategies, and GEA remains a devastating disease worldwide[9].

Transcriptional dysregulation of genes is a hallmark of tumors, and these dysregulated genes can serve as targets for the development of cancer therapeutic drugs[10]. Transcription program activation is triggered by master transcription factors (TFs)[11]. TFs are drivers in cancer and attractive potential targets for tumor therapy because of their core importance to biological functions[12]. In contrast to certain kinase-related proteins (such as EGFR, VEGFR, and BTK), abnormally expressed TFs (except for the nuclear receptor family) lack allosteric regulatory sites and small-molecule binding pockets[13], which makes the development of small-molecule inhibitors targeting TFs extremely challenging. Hence, identifying the biological functions and regulatory mechanisms of abnormally expressed TFs in tumors is clearly important, and screening new antitumor drugs targeting specific TFs and transcription protein complexes has the potential to facilitate the clinical treatment of GEA.

As an epithelial-specific ETS-like factor, ETS homologous factor (EHF) was identified as an EAC-specific master TF[14,15]. EHF is in the ETS transcription factor family[16,17] and has been found to present opposite biological functions in certain cancer types[18,19]. Notably, TFs interact with cofactors to regulate the expression of genes[20], and the multifaceted functions of EHF may be based on its molecular partner—a transcriptional cofactor. In this study, we investigated the biological functions and transcriptional regulatory mechanisms of the dysregulated TF EHF in GEA. Furthermore, we explored the therapeutic potential of targeting EHF and its coactivator, Ajuba LIM protein (AJUBA, also known as JUB), through treatment with polymeric nanoparticles (NPs) encapsulating short interfering RNA (siRNA).

2. Materials and methods

2.1. GEA cell lines and reagents

The EAC cell lines OE33, SKGT4, JH-ESOAD1 and OACP4C were provided by Dr. Jian Pan from the Children's Hospital of Soochow University, and the GAC cell lines HGC-27, MKN28 and MKN45 were maintained and used in our laboratory. The GAC cell line AGS was purchased from FuHeng BioLogy (Shanghai, China). These cell lines were grown in RPMI-1640 medium (Gibco, USA), F12K medium (Gibco, USA), or DMEM (Gibco, USA) supplemented with 10%−20% fetal bovine serum (ExCell Biology, China), 100 U/mL penicillin and 100 ng/mL streptomycin in 5% CO_2 at 37 °C. GEA cell lines were verified by short tandem repeat (STR) analysis and validated to be free of mycoplasma.

2.2. SiRNA transfection

SiRNAs targeting EHF or AJUBA and a negative control (NC) were purchased from GenePharma (Shanghai, China) and transfected into GEA cell lines by RNAiMAX reagents (Invitrogen, USA). The siRNA sequences are listed in Supporting Information Table S1.

2.3. Cell counting kit-8 (CCK-8) assay

Cells were seeded into 96-well plates and then cultured for 1, 3 and 5 days before the addition of 10 μL of CCK-8 solution (Dojindo, Japan) to each well. After the cells were incubated at 37 °C for 2 h, the absorbance was measured at 450 nm with an automatic microplate reader (Spark 10M; TECAN, Switzerland).
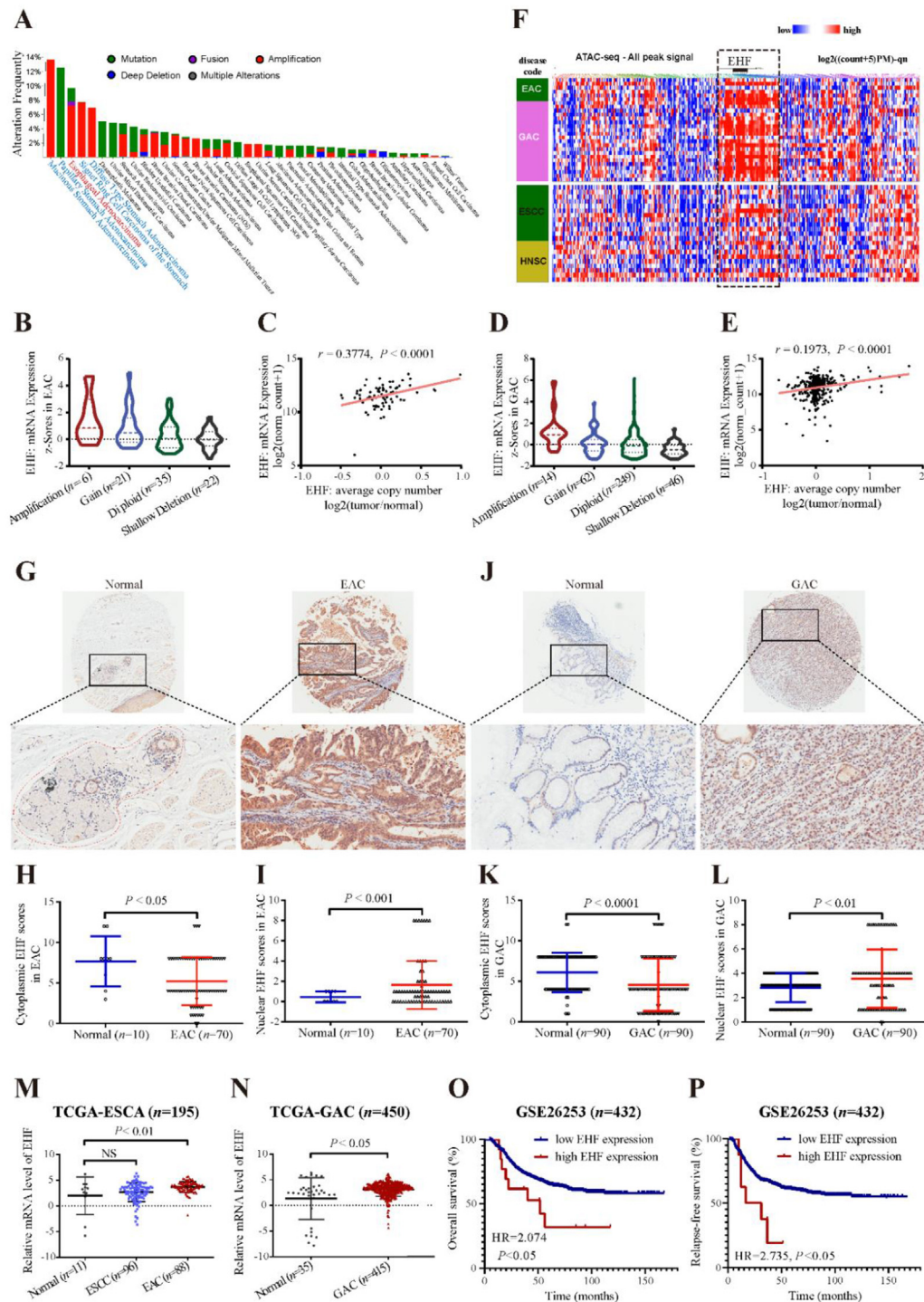
Figure 1 The gene expression, gene alterations and clinical prognostic value of EHF in GEA patients. (A) Alterations in EHF in pan-cancer from cBioPortal for Cancer Genomics. (B) Relative mRNA expression levels of EHF among different types of variations in EAC. (C) Pearson correlation between the copy number and mRNA expression of EHF in EAC. (D) Relative mRNA expression levels of EHF among different types of variations in GAC. (E) The Pearson correlation between the copy number and mRNA expression of EHF in GAC. (F) Chromatin accessibility of EHF in squamous cell carcinoma (SCC) and adenocarcinoma (AC). SCC includes head and neck SCC (HNSCC) and esophageal squamous cell carcinoma (ESCC), and AC includes EAC and GAC. (G) Representative images, (H) cytoplasmic and (I) nuclear EHF immunohistochemistry scores in our EAC tissues. Red dotted circle indicated normal epithelium in 1G. Magnification: 50 or 200×. (J) Representative images, (K) cytoplasmic and (L) nuclear EHF immunohistochemistry scores in our GAC tissues. Magnification: 50 or 200×. Immunohistochemistry images (G, J) were obtained using panoramic scanning and were analyzed using Aperio ImageScope software, which was also utilized to determine the magnification. (M, N) The differential mRNA expression of EHF in (M) esophageal cancer and (N) GAC tumor tissues from the UCSC Xena database. NS, not significant. (O, P) Kaplan−Meier curves were used to assess the relationship between EHF expression and (O) overall survival (OS) or (P) relapse-free survival (RFS) in GAC patients from a Gene Expression Omnibus (GEO) dataset. We used the optimal cutoff value, which was determined by X-tile software[24], to divide patients into two groups.

2.4. 5-Ethynyl-2′-deoxyuridine (EdU) assay

The transfected cells were plated in confocal dishes and incubated with the EdU reagent from a Cell-Light Apollo 567 stain kit (RiboBio, China) for 2 h at 37 °C. Following staining with Apollo 567 and Hoechst 33342 solution, the cells were observed by confocal laser microscopy (CLSM; Zeiss LSM 800 with Airyscan; Zeiss, Germany).

2.5. High-throughput live-cell functional analysis for real-time monitoring of cell numbers

GFP-labeled GEA cells were transfected with siEHF or siNC and then plated in triplicate wells in a 96-well plate. Cells were cultured in a 37 °C chamber and were recorded and numbered every 4 h for two days with a high-throughput live cell functional analysis system (SARTORIUS, IncuCyte S3). The data were analyzed with IncuCyte software.

2.6. Live confocal automated imaging showing the progression of cell mitosis

GEA cells were stably transfected with a pLVX-GFP-H2B lentiviral vector and then transfected with siEHF or siNC. Quintuplicate wells for each group with six fields per well were photographed every 10 min for 48 h with an ImageXpress Micro Confocal imaging system (Molecular Devices, USA).

2.7. Transwell assay

GEA cells were seeded in serum-free medium in upper Transwell chambers, and 500 μL of the corresponding medium containing 20% fetal bovine serum was added to the lower Transwell chambers. After 24 h, the cells were fixed, stained and imaged under an upright microscope (Nikon, Nikon NI-U).

2.8. Cell apoptosis detection

Cells were collected and resuspended in 200 μL of $1\times$ binding buffer and then incubated with 5 μL of Annexin V-FITC and 5 μL of propidium iodide (PI; eBioscience, USA) in each well for 15 min in the dark. The stained cells were detected with a FACSCalibur flow cytometer (BD, USA).

2.9. Quantitative reverse-transcription polymerase chain reaction (qRT-PCR)

Total RNA was extracted from the indicated cells using an RNA Quick Purification kit (ES Science, China) and reverse-transcribed into cDNA with a RevertAid First Strand cDNA Synthesis kit (Thermo Fisher Scientific, USA). qRT-PCR was performed using LightCycler 480 SYBR Green I Master Mix (Roche, Switzerland). All qRT-PCR data were analyzed by the $2^{-\Delta\Delta Ct}$ method. The primer sequences used are listed in Supporting Information Table S2.

2.10. Immunoblotting

Total protein was solubilized in the RIPA lysis buffer and quantified with a BCA protein assay kit (CWBIO, China). The extracted proteins were transferred onto PVDF membranes, which were then incubated with the indicated primary antibodies dissolved in Western primary antibody diluent (Beyotime, China) at 4 °C overnight and then incubated with the corresponding secondary antibodies. The membrane was finally incubated using either a chemiluminescence detection kit (Proteintech, China), a SuperSignal West Femto Maximum Sensitivity Substrate (Thermo Fisher Scientific, USA), or a combination of both. Information on the primary and secondary antibodies used in this study is listed in Supporting Information Table S3.

2.11. Immunofluorescence (IF)

Cells were seeded on confocal films and fixed for IF staining. After being permeabilized and blocked, the cells were probed with the indicated primary antibody overnight at 4 °C and subsequently with fluorescent conjugated secondary antibody in the dark. Following immunostaining, the cells were counterstained with DAPI (Beyotime, China). The stained cells were observed under a confocal laser scanning microscope (Zeiss LSM 800 with Airyscan, Germany).

2.12. Patient-derived xenograft (PDX) model

All animal experiments were carried out according to the guidelines for animal ethics and welfare. All animal experiments were approved by the Animal Welfare and Ethics Committee of Guangzhou Forevergen Biosciences. Human GAC tumor samples were acquired from patients undergoing surgical resection at Sun Yat-sen Memorial Hospital (Guangzhou, China) with written informed consent from patients, which was approved by the Institutional Review Board of the Sun Yat-sen Memorial Hospital of Sun Yat-sen University. Each tumor was promptly cut into small pieces and subcutaneously inoculated into the flanks of anesthetized NOD/SCID/Rag2$^{-/-}$ IL2rg$^{-/-}$ (NSG) mice to construct a first-generation PDX model. When the tumors had grown to less than the size required by the animal ethics guidelines, the xenograft tumors were harvested and sub-transplanted into the next generation of NSG mice following the same protocols used for transplantation in generation 1 mice. Tumor size was examined twice every week and calculated using Eq. (1):

$$V \ (\text{mm}^3) = (L \times W^2)/2 \qquad (1)$$

where L represents the length of the tumor, W represents the width of the tumor.

When the tumor size reached 50−100 mm^3, the mice were randomly allocated into seven groups based on tumor sizes and mouse weights. These seven groups were injected with vehicle (PBS), blank NPs (NPs), siNC-encapsulated NPs (NPs_siNC), siEHF-encapsulated NPs (NPs_siEHF), siAJUBA-encapsulated NPs (NPs_siAJUBA), siEHF combined with siAJUBA-encapsulated NPs (NPs_siEHF+siAJUBA) or oxaliplatin via tail vein injection. Oxaliplatin was used as the positive control. After tumor development, tumor tissues and certain important internal organs, namely, the heart, liver, spleen, lung and kidney, were harvested from the mice for further study.

2.13. Immunohistochemical staining

Two commercial tissue arrays (gastric cancer and esophageal adenocarcinoma) were respectively purchased from OUTDO (SHANGHAI OUTDO BIOTECH) and Tissue Array (TissueArray.Com LLC). Immunohistochemical (IHC) analysis on
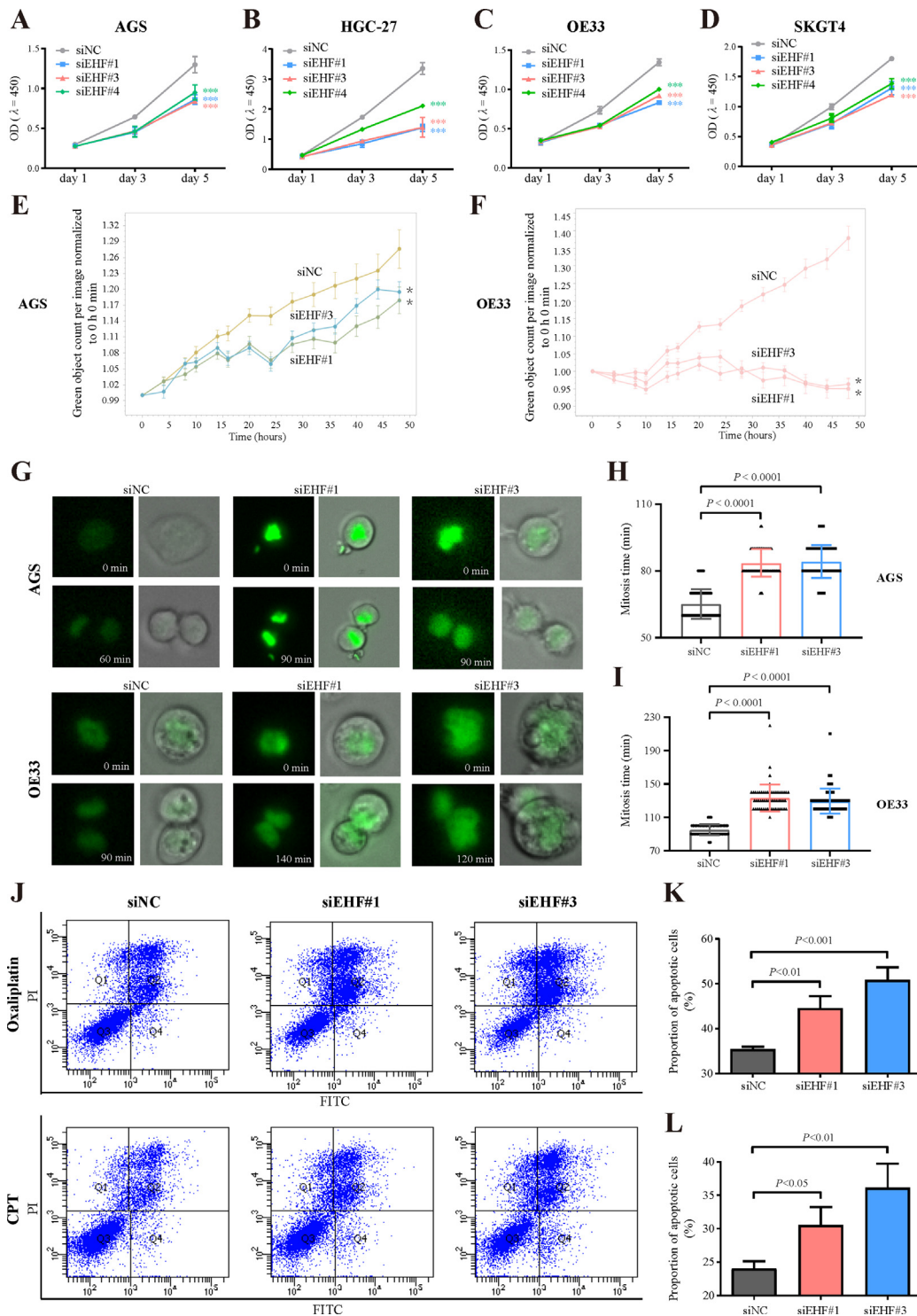
Figure 2 The effect of EHF interference on the viability, mitosis and apoptosis of GEA cells. (A, B) Cell viability was measured using a CCK-8 assay in GAC cell lines (AGS and HGC-27) transfected with siRNA against EHF (siEHF#1, #3 or #4) or siNC. (C, D) Cell viability was measured using a CCK-8 assay in EAC cell lines (OE33 and SKGT4) transfected with siEHF or siNC. (E, F) GFP-labeled AGS and OE33 cells transfected with siEHF or siNC were monitored in real time using a high-throughput live cell functional analysis system. (G) Representative mitotic images and (H, I) mitosis time of AGS and OE33 cells cotransfected with a pLVX-GFP-H2B lentiviral vector and siEHF or siNC. (J−L) Representative images (left) and quantification (right) of apoptotic cells obtained by flow cytometry in GAC cells transfected with siEHF or siNC, each together with oxaliplatin treatment. $*P < 0.05$, $***P < 0.001$.

the samples was performed according to a standard protocol. Briefly, samples were incubated with anti-EHF antibody (GeneTex, GTX116440ab78078; 1:1000 dilution in gastric cancer tissue array, 1:40 dilution in esophageal adenocarcinoma tissue array) as primary antibody, followed by incubation with secondary antibody. The staining scores of cytoplasmic and nuclear EHF were assessed by two independent pathologists.

For the appraisal of morphology, tumors and main internal organs, including the heart, liver, spleen, lung and kidney, were analyzed using hematoxylin and eosin (H&E) staining. To evaluate tumor cell proliferation and apoptosis, tumor tissues were subjected to Ki-67 and TUNEL staining, respectively.

2.14.   Co-immunoprecipitation (co-IP) and mass spectrometry (MS)

Fresh cells were harvested and then incubated with antibodies against EHF or AJUBA bound to Pierce protein A/G magnetic beads (Thermo Fisher Scientific, USA) overnight with rotation at 4 °C. The mixtures were washed and then boiled in $1\times$ SDS loading buffer for 10 min. The input, IgG and immunoprecipitation fractions were analyzed by immunoblotting.

For MS, immunoprecipitated samples were subjected to on-bead peptide digestion and then analyzed using a Thermo Fisher EasyLC 1200-Orbitrap Fusion LC−MS instrument (Thermo Fisher Scientific, USA). The data were processed with Proteome Discoverer software (Version 2.4) by our Bioinformatics and Omics Center.

2.15.   Glutathione S-transferase (GST) pulldown assay

Full-length EHF and AJUBA were synthesized and cloned into a prokaryotic expression vector, GST-tagged pGEX-4T-1 (Igebio, China). The fusion protein with a GST tag was expressed and purified, and the interaction between EHF and AJUBA was detected.

2.16.   RNA sequencing (RNA-seq)

Total RNA was isolated from GEA cells using the classical TRIzol method. An mRNA library was established and then subjected to sequencing by BGIseq500 (BGI-Shenzhen, China).

2.17.   Gene set enrichment analysis

Gene set enrichment analysis (GSEA) based on the HALLMARK gene sets was performed to identify gene sets with significant differences after interfering with EHF or AJUBA expression. The HALLMARKER gene sets (h.all.v6.2.symbols.gmt) obtained from the Molecular Signatures Database (MSigDB; https://www.gsea-msigdb.org/gsea/msigdb/index.jsp) were selected as the reference gene sets.

In addition, GSEA was performed to explore the synergy between EHF and AJUBA expression. siAJUBA and siEHF downregulated gene expression according to our RNA-seq data, and these downregulated genes served as the reference gene sets.

2.18.   Chromatin immunoprecipitation sequencing (ChIP-seq) and analysis

AGS cells were cultured in 150 mm dishes and then crosslinked with 1% formaldehyde for 10 min at room temperature, followed by quenching with 125 mmol/L glycine for 5 min. Crosslinked DNA was sheared to approximately 300−500 bp using a Bioruptor Plus (Diagenode, Belgium) under the condition of 30 s on and 30 s off. Ten percent of the volume of chromatin was kept as input before IP. Chromatin was immunoprecipitated with Pierce protein A/G magnetic beads (Thermo Fisher Scientific, USA) bound with corresponding antibodies at 4 °C overnight. After reverse crosslinking with 5 mol/L NaCl (4 μL per 100 μL of sample volume) at 65 °C overnight using fresh elution buffer, chromatin-immunoprecipitated DNA was purified and subjected to sequencing. Information on the antibodies used for the ChIP assay is listed in Supporting Information Table S3.

Clean ChIP-seq reads with removal of low-quality and adaptor sequences were provided by BGI Genomics. The quality of the clean reads was checked using FASTQC software. ChIP-seq data analysis was performed as previously described[21−23]. Briefly, bowtie2 was used to map ChIP-seq reads into the human reference genome hg19, model-based analysis of ChIP-seq 2 (MACS2) was used to call significant peaks, and integrative genomics viewer (IGV) was used to visualize BigWig files of ChIP-seq. In addition, rank ordering of super-enhancers (ROSE) was used to identify SEs by H3K27ac ChIP-seq.

## 2.19.   Assay for transposase-accessible chromatin and sequencing (ATAC-seq)

AGS cells were stably transfected with PLKO.1-puro short hairpin RNA (shRNA) lentivirus vectors targeting EHF or AJUBA. The shRNA sequences used in this study are listed in Supporting Information Table S4. The indicated live cells were harvested, counted and treated with a cold lysis buffer. A nuclear pellet was acquired and immediately incubated with a transposition reaction mix, which included Tn5 transposase. After purification and PCR amplification, the libraries were sequenced on a BGIseq500 (BGI-Shenzhen, China).

2.20.   Characterization of NPs

Lipid-based NPs coated with the indicated siRNAs were fabricated following the sonication method by Kelanbio. Dynamic light scattering (DLS) and transmission electron microscopy (TEM) were performed to characterize the NPs. The dimensional distribution and zeta potential of the NPs were estimated by DLS (with a Zetasizer Nano ZS, Malvern, UK). Additionally, the morphology and size of the NPs were delineated by TEM (HT7800, Hitachi, Japan).

2.21.   Cellular uptake of the NPs

AGS and OE33 cells were seeded on confocal dishes and incubated overnight. FAM-siNC-coated NPs were added to the attached cells in Opti-MEM (GIBCO, USA). At the same time, FAM-siNC was transfected into cells with vehicle (PBS) and the transfection reagent RNAiMAX (Invitrogen, USA) under the same conditions, and these cells were the negative control and positive control, respectively. After 6 h of incubation at 37 °C with 5% CO_2, the treated cells were stained with phalloidin-iFluor 555 (Abcam, UK) and DAPI (Beyotime, China) and observed with a confocal laser scanning microscope (Zeiss LSM 800 with Airyscan, Zeiss, Germany).
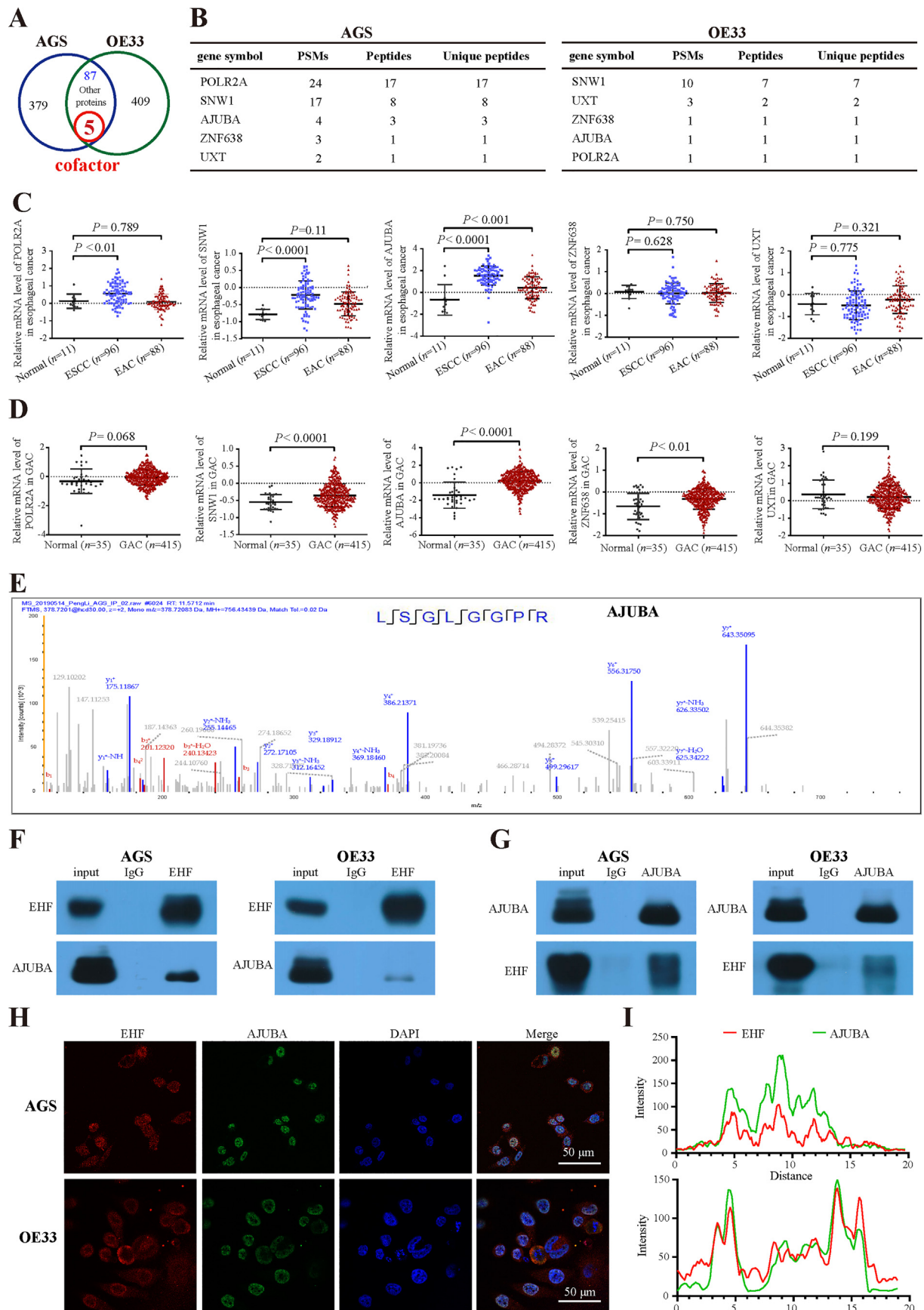
Figure 3 The interaction of TF EHF with cofactor AJUBA in GEA cells. (A) Venn diagram showing the interacting proteins, including co-factors, with TF EHF, as determined *via* co-IP assay combined with MS analysis. (B) Three-line table showing the MS data of five cofactors

2.22. Statistical analysis

All statistical analyses were carried out using SPSS 17.0 (SPSS, USA) and GraphPad Prism 8 (GraphPad, USA) software. Student's *t* test and analysis of variance (ANOVA) were performed to evaluate the differences between two groups and multiple groups, respectively. Pearson correlation coefficient analysis was performed to determine correlations. The Kaplan−Meier method (log-rank test) was used to evaluate the survival of patients. Differences assessed by two-tailed tests were considered statistically significant when $P < 0.05$.

2.23. Data availability

The raw RNA-seq, ChIP-seq and ATAC-seq data generated in this study have been deposited into the public Gene Expression Omnibus (GEO) repository under accession number GSE207556. The RNA-seq data of GEA cells transfected with siRNAs (siEHF, siAJUBA and siNC) were stored in GEO under accession number GSE207553; the ChIP-seq data of GEA cells were stored in GEO under accession number GSE207554; the ATAC-seq data of GEA cells treated with shRNAs (shEHF, shAJUBA and shNC) were stored in the GEO under accession number GSE207555.

3. Results

3.1. EHF is transcriptionally activated, highly expressed and associated with a poor prognosis in GEA patients

EHF was identified as a master TF in EAC in our previous study[15], and master TFs are usually relatively highly expressed in specific tumor types. Here, we evaluated the expression and genetic alteration of EHF across cancers in the Cancer Cell Line Encyclopedia (CCLE) and The Cancer Genome Atlas (TCGA) datasets. EHF was relatively highly expressed in cell lines and tumor samples of GEA, including EAC and GAC, compared with those of other cancers (Supporting Information Fig. S1A and S1B). In addition, EHF showed a higher frequency of genetic alterations, mainly gene amplification, in GEA than in other cancers (Fig. 1A). Next, we observed the effect of different genetic alteration types on EHF mRNA expression. Compared with diploid and shallow deletion, amplification and gain exerted greater effects on EHF expression (Fig. 1B, D). A positive correlation was observed between EHF expression and its copy number in GEA samples (Fig. 1C, E), suggesting that an increased copy number partially explained the overexpression of EHF in the GEA samples. We further examined the methylation of EHF in GEA samples and found no change in this modification between GEA and squamous cell carcinoma tissues (Fig. S1C), indicating that EHF methylation should not explain its upregulated expression in GEA.

Furthermore, we investigated the chromatin accessibility of EHF by ATAC-seq. The chromatin accessibility of EHF regions was relatively high in GEA but relatively low in esophageal, head and neck squamous cell carcinomas (Fig. 1F; Fig. S1C). These results

indicated that EHF transcription was activated in GEA. In addition, the protein expression level of EHF was determined *via* immunohistochemistry assay with GEA samples. Cytoplasmic EHF expression was found to be decreased (Fig. 1G, H), while nuclear EHF expression was found to be increased in our EAC samples (Fig. 1G, I; Supporting Information Fig. S2A−S2C). Similar results were observed with our GAC samples (Fig. 1J−L; Fig. S2D−S2F), providing additional evidence that EHF plays a role in GEA after entering the nucleus. Moreover, an analysis of public TCGA datasets showed that the mRNA expression of EHF was upregulated in EAC and GAC patients (Fig. 1M, N; Fig. S2G, S2H). Importantly, Kaplan−Meier curve analysis clearly showed that high EHF expression indicated lower overall survival (OS) and relapse-free survival (RFS) than low EHF expression (Fig. 1O, P).

3.2. EHF interference inhibited cell viability and migration and promoted the apoptosis of GEA cells

To evaluate the biological role of EHF in GEA carcinogenesis, the efficiency of EHF interference was validated in eight GEA cell lines *via* qRT-PCR (Supporting Information Fig. S3A−S3H) and immunoblotting (Fig. S3I−P). In this experiment, four GAC cell lines (AGS, HGC-27, MKN28 and MKN45) and four EAC cell lines (OE33, SKGT4, JH-ESOAD1 and OACP4C) were tested. We next detected the effect of EHF knockdown on the proliferation, apoptosis and migration of GEA cells. CCK-8 assays showed that knockdown of EHF expression by siRNA decelerated cell growth in GAC (Fig. 2A, B; Supporting Information Fig. S4A, S4B) and EAC cells (Fig. 2C, D; Fig. S4C, S4D). Consistent with the CCK-8 assay results, an automatic live-cell imaging system showed that EHF interference slowed cell proliferation (Fig. 2E, F) and lengthened the mitosis of GEA cells (Fig. 2G−I). Furthermore, flow cytometry showed that EHF interference led to an increase in apoptosis of GEA cells (Supporting Information Fig. S5A−S5D). At the same time, camptothecin (CPT) or oxaliplatin induced cell apoptosis (Supporting Information Fig. S6A−S6D), and EHF interference led to an increase in apoptotic cells induced by CPT or oxaliplatin (Fig. 2J−L, Supporting Information Fig. S7A−S7D). Also, we observed an upregulation in the expression of apoptotic marker proteins following siEHF treatment, further adding to the evidence of EHF interference's pro-apoptotic role in GEA cells (Supporting Information Fig. S8A, S8B). Additionally, Transwell assays indicated that EHF interference decreased the migratory ability of GAC and EAC cells (Fig. S4E). These results suggested that EHF interference reduced cell viability and inhibited mitosis and migration while increasing the apoptosis rate of GEA cells.

3.3. EHF expression is upregulated by a CRC (ELF3-KLF5-GATA6) in GEA

In our previous study, we identified a CRC formed by four master TFs, E74-like ETS transcription factor 3 (ELF3), KLF transcription factor 5 (KLF5), GATA binding protein 6 (GATA6) and EHF, in EAC[15]. In this study, the transcriptional regulation of ELF3,

---

(POLR2A, SNW1, AJUBA, ZNF638 and UXT) interacting with EHF in AGS and OE33 cells. (C, D) The mRNA expression levels of POLR2A, SNW1, AJUBA, ZNF638 and UXT in esophageal carcinoma (EC) and GAC samples. (E) The mass spectrum of AJUBA. (F) The protein interaction of EHF with cofactor AJUBA in AGS and OE33 cells as determined by endogenous co-IP coupled with immunoblotting. (G) The protein interaction of cofactor AJUBA with EHF in AGS and OE33 cells by endogenous co-IP coupled with immunoblotting. (H, I) Immunofluorescence labeling with an anti-EHF antibody (red) or anti-AJUBA antibody (green) and counterstaining with DAPI (blue), showing the colocalization of TF EHF and cofactor AJUBA in AGS and OE33 cells as determined by CLSM. Scale bar: 50 μm.
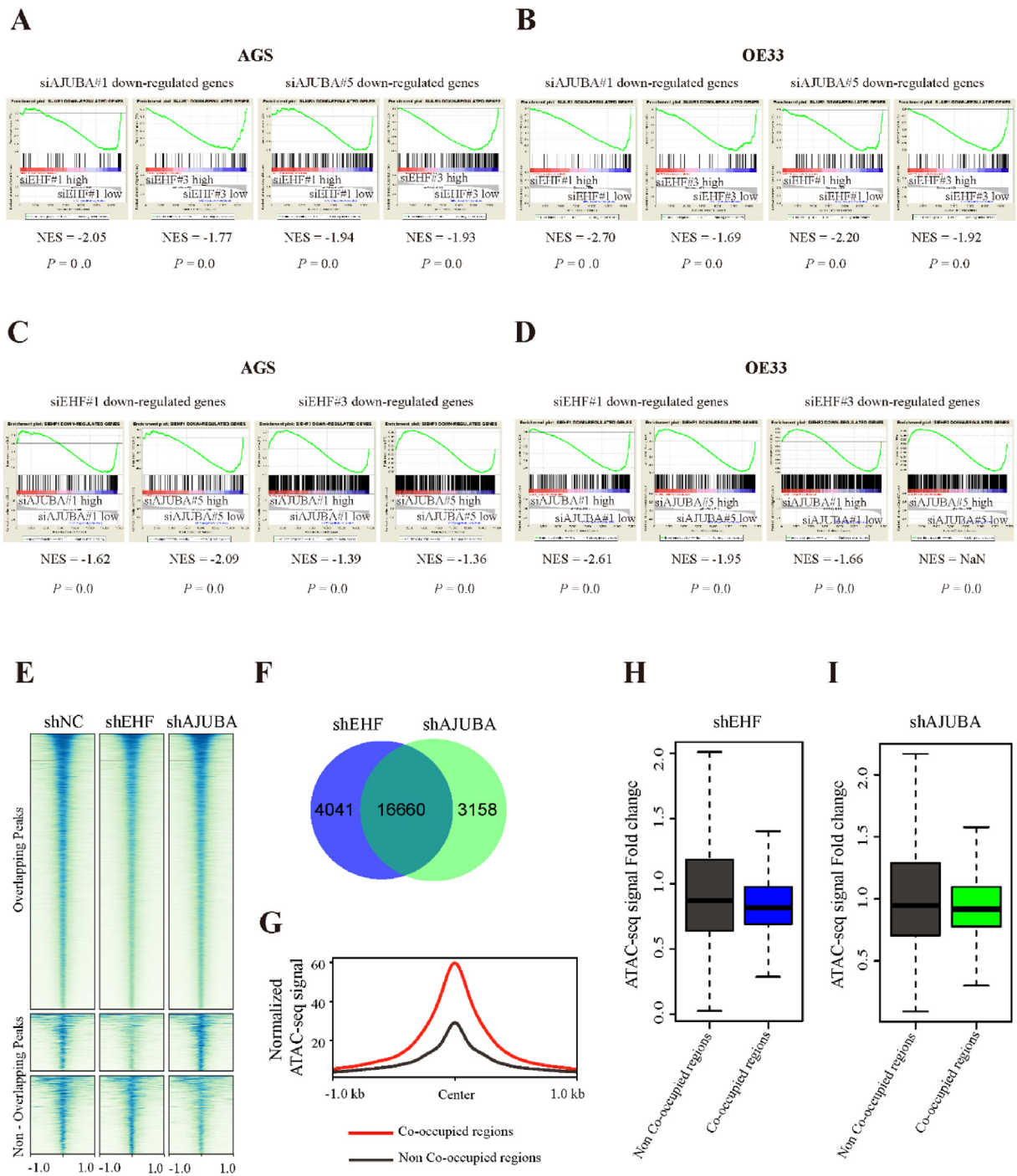
Figure 4 The transcriptional cooperativity between EHF and coactivator AJUBA. (A, B) GSEA showed that genes downregulated by EHF siRNAs (siEHF#1 and #3) were significantly enriched in the downregulated gene set after AJUBA interference in AGS and OE33 cells. (C, D) GSEA plots showed that genes downregulated by AJUBA siRNAs (siAJUBA#1 and #5) were significantly enriched in the downregulated gene set following EHF interference in AGS and OE33 cells. NES, normalized enrichment score. (E) ATAC-seq heatmaps revealing genome-wide signals after EHF or AJUBA interference by short hairpin RNA (shEHF or shAJUBA) in AGS cells, ranked by the signal intensity. shNC served as the control group. These regions were further stratified into overlapping and nonoverlapping regions. (F) Venn diagram showing shared and exclusive genomic regions as determined by ATAC-seq signal analysis after interference of EHF or AJUBA. (G) Comparison of normalized ATAC-seq signals between co-occupied regions and non-co-occupied regions from EHF and AJUBA. (H, I) ATAC-seq signal fold change in the co-occupied and non-co-occupied regions after interference of EHF and AJUBA.
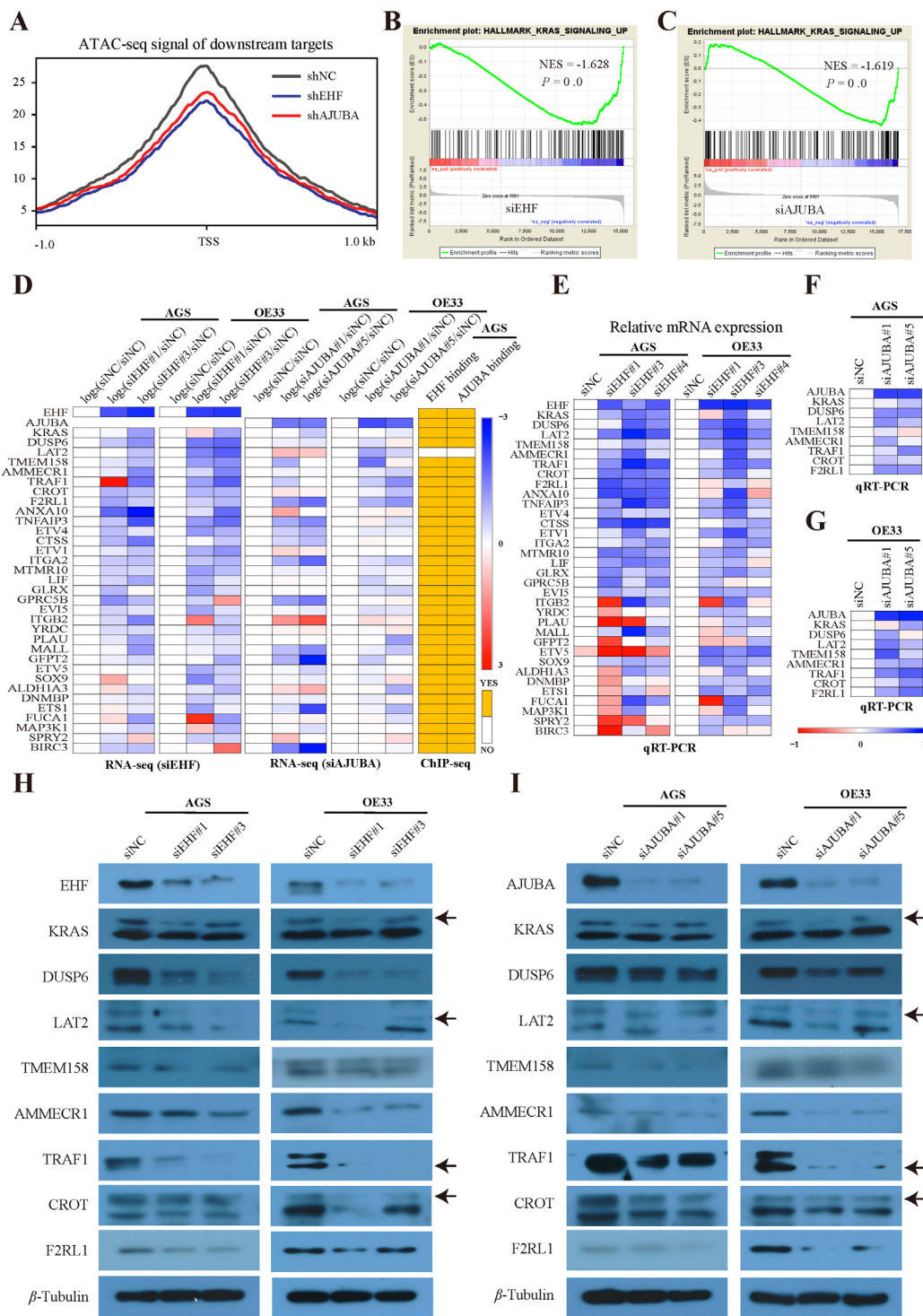
Figure 5 EHF and AJUBA cooperate to promote KRAS pathway signaling in GEA cells. (A) ATAC-seq signals of downstream genes in AGS cells transfected with shRNA against EHF and AJUBA. (B, C) GSEA plots showing the enrichment of KRAS signaling in AGS cells after EHF and AJUBA interference. (D) Heatmaps displaying the mRNA expression of KRAS signaling-related genes in AGS and OE33 cells transfected with siRNA against EHF (siEHF) or AJUBA (siAJUBA), as determined with RNA-seq data (left), and the binding of KRAS signaling-related genes with EHF and AJUBA, as determined by the respective ChIP-seq data (right). (E) qRT-PCR showing the mRNA expression levels of KRAS signaling-related genes in AGS cells (left) and OE33 cells (right) transfected with siEHF. (F, G) qRT-PCR determination of the mRNA expression levels of KRAS signaling-related genes in AGS and OE33 cells transfected with siAJUBA. (H, I) Immunoblotting showing the protein content of KRAS signaling-related genes after transfection of siRNA against EHF (left) and AJUBA (right) in AGS and OE33 cells.

KLF5, GATA6 and EHF was observed in GEA. First, we inspected the expression correlation of these four master TFs at the mRNA level and verified that the expression of the four candidate genes ELF3, KLF5, GATA6 and EHF showed a significantly positive correlation with each other in EAC tissues in a GEO dataset (Supporting Information Fig. S9A) and TCGA database (Fig. S9B). Similar results were found in GAC samples (Fig. S9C−S9F). To validate the interconnected transcriptional regulation of these genes, siRNAs were used to interfere with the expression of each of the master TFs. Knocking down the expression of TFs ELF3, KLF5 or GATA6 led to downregulated mRNA expression of the three TF genes and EHF, as indicated by qRT-PCR (Fig. S9G, S9H). Consistent with the qRT-PCR data, the protein expression levels of ELF3, KLF5, GATA6 and EHF decreased in AGS and OE33 cells transfected with siRNAs of the three TF genes (Fig. S9I, S9J). Moreover, the overexpression of ELF3, KLF5, or GATA6 demonstrated similar results, further validating their mutual regulatory interplay forming a CRC and upregulating EHF expression (Supporting Information Fig. S10A, S10B). Additionally, both ChIP-seq and ChIP-qPCR results consistently showed the upregulatory effects of ELF3, KLF5, or GATA6 on EHF, highlighting their modulating roles on EHF expression (Supporting Information Fig. S11A−S11F). However, with the knockdown of EHF expression, the expression of ELF3, KLF5 and GATA6 was not decreased in GAC cells, as indicated by RNA-seq, qRT-PCR and immunoblotting (Supporting Information Fig. S12A−S12F). These results indicated that the three master TFs, ELF3, KLF5 and GATA6, form a CRC in GEA, and this CRC upregulates EHF. In addition, according to the pan-cancer RNA-seq data obtained from both the TCGA and CCLE samples, the candidates ELF3, KLF5 and GATA6 were generally highly expressed in EAC and GAC samples compared to most other tumor types (Supporting Information Fig. S13A−S13F).

3.4. AJUBA is a novel cofactor of EHF in GEA cells

Most eukaryotic transcription factors generally do not act alone but perform their functions by interacting with cofactors[25,26]. To identify the cofactors that interact with TF EHF, a co-IP assay combined with MS analysis was performed. A total of 97 EHF-interacting proteins were identified in both AGS and OE33 cells, of which five were cofactors (POLR2A, SNW1, AJUBA, ZNF638 and UXT) (Fig. 3A, B). We next analyzed the expression of these five cofactors in GEA tissues. A prominent increase was observed in the expression of AJUBA, but not in the expression of POLR2A, UXT, SNW1 or ZNF638, in both the EAC (Fig. 3C) and GAC samples (Fig. 3D). Based on the above results, we chose cofactor AJUBA for further study (Fig. 3E). A co-IP assay followed by immunoblotting validated the EHF interaction with AJUBA in AGS and OE33 cells (Fig. 3F). Moreover, AJUBA was found to interact with EHF (Fig. 3G). Similar results were observed by GST pull-down assays (Supporting Information Fig. S14A, S14B). Colocalization of EHF and AJUBA in the nucleus of AGS and OE33 cells was observed by immunofluorescence assay (Fig. 3H, I). These data suggested that EHF interacts with cofactor AJUBA in the nucleus of GEA cells.

3.5. Transcriptional cooperativity between EHF and its coactivator AJUBA

The activity of enhancers is mediated through the binding of TFs and cofactors[27,28]. To observe the cooperative effects between the master TF EHF and its cofactor AJUBA on transcription, we first performed RNA-seq with AGS and OE33 cells transfected with siEHF or siAJUBA (Supporting Information Fig. S15A− S15H). GSEA based on the RNA-seq data obtained from AGS cells showed that the genes decreased following EHF knockdown were significantly enriched in a gene set downregulated upon AJUBA knockdown (Fig. 4A). The same method was used with the RNA-seq data obtained from OE33 cells (Fig. 4B). Similarly, the genes with reduced expression after AJUBA silencing were prominently enriched in a set of genes downregulated upon EHF interference in AGS (Fig. 4C) and OE33 cells (Fig. 4D).

To further explore whether EHF and its newly identified cofactor AJUBA cooperatively affect chromatin accessibility, ATAC-seq was carried out with AGS cells in which EHF or AJUBA expression had been knocked down. Notably, 69.83% of the lost peaks in AGS cells overlapped following knockdown of EHF or AJUBA (Fig. 4E, F), suggesting that these two factors comodulated the accessibility of tens of thousands of cis-regulatory regions across the genome. In addition, the enhancer regions occupied in both EHF and AJUBA showed considerably greater accessibility (Fig. 4G). Importantly, interference of EHF or AJUBA expression markedly decreased the ATAC-seq signals in the co-occupied regions compared with the non-co-occupied regions (Fig. 4H, I). These ATAC-seq data indicated that the alteration of chromatin accessibility was a result of transcriptional cooperativity between TF EHF and its cofactor AJUBA. Collectively, the above results demonstrated that the master TF EHF and its coactivator AJUBA orchestrate the identified transcriptional network in GEA cells.

3.6. EHF and AJUBA cooperate to promote the KRAS signaling pathway in GEA cells

Combined analysis of RNA-seq data and ATAC-seq data showed that the ATAC-seq signal of downregulated downstream genes also decreased significantly after EHF and AJUBA knockdown (Fig. 5A). To determine downstream signaling molecules co-regulated by EHF and AJUBA, GSEA based on the RNA-seq analysis data obtained from GEA cells with EHF or AJUBA interference was performed. KRAS signaling was conspicuously downregulated in the AGS and OE33 cells upon silencing of either EHF or AJUBA (Fig. 5B, C). Focusing on the constituents of KRAS signaling, we chose 33 genes with downregulated expression upon EHF and AJUBA knockdown (Fig. 5D). ChIP-Seq data showed that more than 95% of these 33 downregulated genes were directly occupied by TF EHF or its cofactor AJUBA (Fig. 5D), validating that the alterations in the expression of these genes were caused by direct transcriptional regulation. Moreover, the genes that were downregulated in the KRAS signaling pathway were concurrently occupied by EHF and AJUBA (Fig. 5D), providing evidence of transcriptional cooperativity between EHF and AJUBA.

To confirm the regulatory effect of EHF and AJUBA on the KRAS pathway, the downregulated genes in the KRAS signaling pathway were first examined by qRT-PCR following siRNA targeting of EHF or AJUBA in AGS and OE33 cells. Among the candidate downregulated genes in the RNA-seq data, eight genes (KRAS, DUSP6, LAT2, TMEM158, AMMECR1, TRAF1, CROT and F2RL1) were confirmed by qRT−PCR (Fig. 5E−G). Then, immunoblotting verified that the protein expression levels of these eight genes were also downregulated (Fig. 5H, I). Furthermore, we
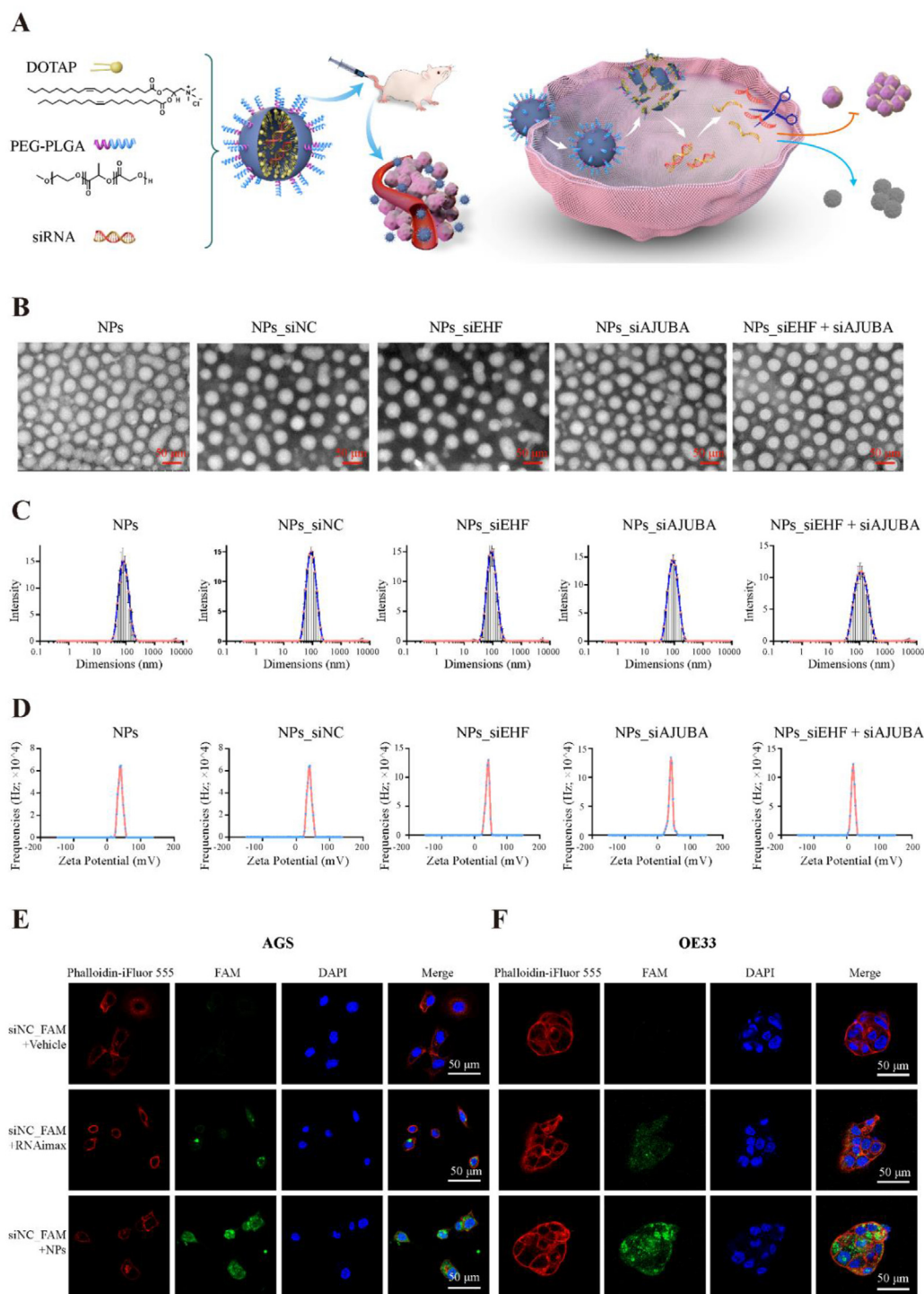
Figure 6 Composition and characterization of NPs with encapsulated siRNA against EHF (siEHF) or AJUBA (siAJUBA). (A) Molecular constitution and schematic interpretation of the lipid-based NP platform for the delivery of siRNA as a GEA treatment. (B) Morphology of blank NPs after treatment with different siRNA-encapsulated NPs (NPs_siNC, NPs_siEHF, NPs_siAJUBA, and NPs_siEHF+siAJUBA), as determined by TEM with corresponding images. Scale bars: 50 μm. (C) Dimension distribution of blank NPs and different siRNA-encapsulated NPs, as determined by DLS. (D) Zeta potential of the blank NPs and different siRNA-encapsulated NPs, as determined by DLS. (E, F) CLSM images displaying the cellular uptake of siRNA_FAM in AGS and OE33 cells. Cells were incubated with free siRNA_FAM or siRNA_FAM-encapsulated NPs in a 37 °C incubator for 6 h. siRNA_FAM transfected with RNAiMAX was the positive control. Membranes were stained with phalloidin-iFluor 555 (red signal), and nuclei were stained with DAPI (blue signal). Scale bar: 50 μm.

examined the impact of EHF or AJUBA knockdown on the downstream protein levels of KRAS, pMEK and pERK and found that EHF or AJUBA knockdown reduced pMEK1/2 levels but had no significant effect on pERK1/2 levels (Supporting Information Fig. S16A, S16B). In addition, KRAS inhibitors exhibited similar effects to EHF and AJUBA silencing (Supporting Information Fig. S17A−S17G).

3.7. Characterization of siEHF- and siAJUBA-encapsulated NPs

Targeting TFs, except for TFs in the nuclear receptor family, with small molecules is challenging[29] since these TFs do not have an active pocket. Nanotechnology has revolutionized the therapy of many diseases, including cancers[30], and has gradually attracted attention because of the effective mRNA vaccines that were developed to combat COVID-19[31]. In this study, a polymeric NP system consisting of the FDA-approved polymer polyethylene glycol (PEG)-poly(lactic-co-glycolic acid) (PLGA) and the cationic lipid 1,2-dioleoyl-3-trimethylammonium propane (DOTAP) (Fig. 6A) was used to deliver siRNA into tumor cells. After encapsulating siRNA, NP size and zeta potential were determined by TEM and DLS. The siRNA-encapsulated NPs were well-defined spheroidal nanostructures (Fig. 6B), with an average hydrodynamic diameter and zeta potential of ∼58.8 nm (Fig. 6C) and 20.6 mV (Fig. 6D), respectively.

Efficient cellular uptake of siRNA is a prerequisite for siRNA-mediated genetic silencing[32]. However, the cell membrane is a well-characterized barrier to siRNA delivery. Therefore, we assessed the uptake of siRNA-encapsulated NPs by GEA cells. NPs were loaded with scramble siRNA marked with the fluorescent label FAM (NPs_siNC-FAM), and the cell-internalized NPs were visualized with CLSM. Cells treated with free siNC-FAM (the negative control) showed a negligible fluorescent signal, but cells transfected with transfection reagents (the positive control) emitted a strong signal (Fig. 6E, F), as expected. Importantly, a strong fluorescent signal was observed in cells incubated with NPs_siNC-FAM (Fig. 6E, F), demonstrating successful cellular uptake of the siRNA-encapsulated NPs by GEA cells in vitro. We further explored whether siRNA-encapsulated NPs were enriched at tumor sites in vivo. NPs_siNC-FAM were first injected into tumor-free and tumor-bearing mice through the tail vein. The mice were then anesthetized after different treatment durations (1 and 24 h), and the fluorescence distribution in the mice in vivo was observed with an optical imaging system designed for small animal studies (IVIS Spectrum imaging; Supporting Information Fig. S18A, S18B). The mice were sacrificed after 24 h, the main organs and tumor tissue were isolated, and the fluorescence intensity of NPs_siNC-FAM was detected by IVIS Spectrum imaging (Fig. S18C). These results indicated that siRNA-encapsulated NPs injected through the tail vein were enriched at the tumor site in vivo.

3.8. siEHF- and siAJUBA-encapsulated NPs cooperate to repress GEA malignancy in vitro and in vivo

After validating the effective internalization of siRNA-encapsulated NPs in target cells, the gene silencing efficacy and therapeutic potential in tumors were determined at the cellular and PDX levels. We first detected the interference effects of siEHF- and siAJUBA-encapsulated NPs in GEA cells. NPs encapsulating siEHF and siAJUBA prominently knocked down the expression of EHF and AJUBA in GEA cells at both the mRNA and protein levels (Supporting Information Fig. S19A−S19D). To directly confirm that EHF and AJUBA can be potential therapeutic targets for the treatment of GEA, the proliferation of GEA cells following treatment with siEHF- or siAJUBA-encapsulated NPs was examined by both EdU and CCK-8 assays. Treatment with either siEHF- or siAJUBA-encapsulated NPs observably inhibited the proliferation of GEA cells compared with that of GEA cells internalizing siNC-encapsulated NPs (Fig. S19E, S19F). Taken together, these data verified that both siEHF and siAJUBA delivered by NPs substantially decelerated GEA cell growth in vitro.

Encouraged by the therapeutic efficacy observed in vitro, we further evaluated the in vivo therapeutic performance of siEHF- and siAJUBA-encapsulated NPs in a PDX model. We established a treatment protocol on the basis of previously published studies that involved a repetitive three-day regimen (Fig. 7A). When tumors reached 50−100 mm^3, mice received either vehicle (PBS), blank NPs, siNC-encapsulated NPs (NPs_siNC), siEHF-encapsulated NPs (NPs_siEHF), siAJUBA-encapsulated NPs (NPs_siAJUBA), siEHF-encapsulated NPs combined with siAJUBA-encapsulated NPs (NPs_siEHF+siAJUBA) or oxaliplatin (positive control) treatment. Unsurprisingly, the positive control PDX model group, which was treated with oxaliplatin, showed a markedly decreased tumor burden (Fig. 7B, C). Consistent with our in vitro experiment, siEHF-encapsulated NPs, siAJUBA-encapsulated NPs and siEHF-encapsulated NPs combined with siAJUBA-encapsulated NPs efficiently decelerated tumor growth compared to the effect of siNC-encapsulated NPs (Fig. 7B, C; Supporting Information Fig. S20A). Importantly, the most striking effect was observed for the combination group of siEHF- and siAJUBA-encapsulated NPs (Fig. 7B, C).

Additionally, the body weights of the mice did not vary notably among all groups (Fig. S20B), indicating an absence of toxicity. H&E staining was employed to evaluate the architectural integrity of the main internal organs. No obvious pathological alterations in the architecture of the main internal organs, including heart (Fig. S20C), liver (Fig. S20D), spleen (Fig. S20E), lung (Fig. S20F) or kidney (Fig. S20G), were observed in the mice treated with vehicle (PBS), blank NPs, or any of the siRNA-encapsulated NPs, demonstrating that no visible adverse side effects manifested in these tissues. H&E staining obviously showed nests of neoplastic cells in the tumors of each group (Fig. 7D). Furthermore, Ki67 and TUNEL staining showed that siEHF-encapsulated NPs, siAJUBA-encapsulated NPs, siEHF- combined with siAJUBA-encapsulated NPs and oxaliplatin all decreased the number of proliferating cells (Fig. 7E) and increased the number of apoptotic cells (Fig. 7F). In summary, the results demonstrated that interference with EHF and AJUBA expression mediated by NPs led to synergistic antitumor effects in GEA both in vitro and in vivo.

Furthermore, we extended our investigation to the impact of siEHF- and siAJUBA-encapsulated NPs on KRAS pathway signaling in GEA cells. Our findings revealed that these NPs effectively downregulated the mRNA and protein levels of key genes in the KRAS pathway (Supporting Information Fig. S21A−S21D). These results not only align with our earlier observations on the influence of siEHF and siAJUBA on the KRAS pathway (Fig. 5) but also further illuminate the underlying molecular mechanisms, reinforcing the potential of EHF and AJUBA as valuable molecular targets in GEA therapy.
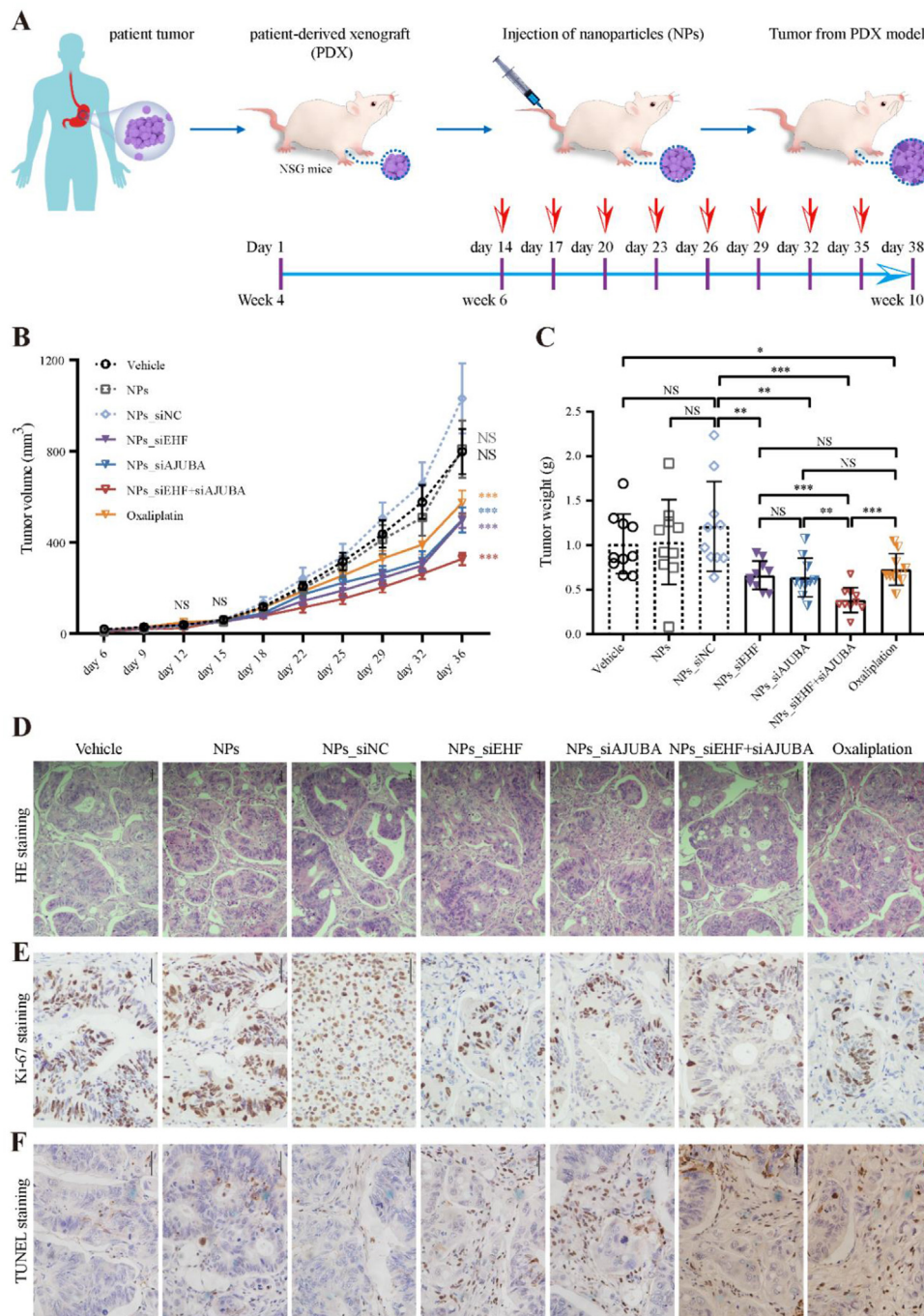
Figure 7   siEHF- and siAJUBA-encapsulated NPs cooperate to repress GEA development in PDX models. (A) Schematic formulation of tumor xenograft establishment and therapy map of the PDX model. Groups of NSG mice were treated with PBS (vehicle), blank NPs (NPs), siNC-encapsulated NPs (NPs_siNC), siEHF-encapsulated NPs (NPs_siEHF), siAJUBA-encapsulated NPs (NPs_siAJUBA) or siEHF- and siAJUBA-encapsulated NPs (NPs_siEHF+siAJUBA) by tail intravenous injection (40 mg/kg, once every three days). NPs_siNC (tail intravenous injection, isovolumetric among groups, once every three days) was used as the negative control. Oxaliplatin (tail intravenous injection, 5 mg/kg, once every three days) was used as the positive control. (B) Growth curves of the tumors from the PDX mice in each group; $n = 10$. The data are presented as the means $\pm$ SEM, $*P < 0.05$, $**P < 0.01$, $***P < 0.001$; NS, not significant. (C) Tumor weight of the PDX mice in each group, $n = 10$. The data are presented as the means $\pm$ SEM, $*P < 0.05$, $**P < 0.01$, $***P < 0.001$; NS, not significant. (D) Representative H&E staining of tumor samples from the PDX mice in the respective groups. Scale bar: 100 μm. (E) Representative images of Ki-67 staining of tumor samples from the PDX model mice in each group. Scale bar: 100 μm. (F) Representative photos of TUNEL staining of tumor samples from the PDX model mice in each group. Scale bar: 100 μm.

4. Discussion

Transcription factors are of interest in medicine because of their importance in gene transcription and biological processes. As an epithelial-specific ETS-like factor, EHF binds to the enhancer or promoter of target genes through its purine-rich GGAA/T core motif. Here, we observed the expression, alteration and chromatin accessibility of EHF and found that EHF was relatively highly expressed and showed higher variations in frequency and transcriptional activity in GEA. These results are in accordance with the property of EHF as a master TF in GEA. EHF has been investigated as a carcinogenic factor in lung adenocarcinoma[33], gastric cancer[34] and intestinal cancers[18], while it has also been found to play a cancer-suppressive role in pancreatic cancer[35,36], head and neck squamous cell carcinoma (HNSCC)[37] and oral squamous cell carcinoma (OSCC)[38]. In the current study, the mRNA and protein expression levels of EHF were upregulated in GEA, and high EHF expression indicated a poor prognosis for GAC patients. Moreover, EHF promoted cell viability and cell migration and suppressed cell apoptosis in GEA. These results all point to EHF as a cancer-promoting molecule in GEA.

Most TFs do not work alone. TFs can form an interregulatory circuit by binding to their own super-enhancers (SEs) and can also form an interconnected loop with other master TFs and their SEs, a program termed the CRC[27,39,40]. Previous studies have identified certain CRCs in multiple cancer types, such as Ewing sarcoma[11], esophageal squamous cell carcinoma (ESCC)[41] and EAC[15]. We previously revealed that four master TFs, EHF, ELF3, KLF5 and GATA6, form a CRC by interacting with the SEs of each other in EAC[15], and another group identified a CRC formed by three TFs, ELF3, EHF and TGIF1, in lung adenocarcinoma[33]. However, no CRC in gastric cancer or GEA has been characterized to date. In addition, EHF has been reported to regulate gene expression by maintaining enhancer-promoter connections and a chromatinic state[42], indicating the involvement of EHF in transcriptional dysregulation. Therefore, we tried to discern whether the expression of the master TF EHF was increased in GEA from the perspective of transcriptional regulation. We characterized a CRC formed by the master TFs ELF3, KLF5 and GATA6 in GEA and found that EHF was transcriptionally activated through this CRC loop. Of note, ELF3 contributed to the formation of CRC in several adenocarcinomas, including EAC, lung adenocarcinoma and GAC. ELF3 plays a vital role in the occurrence and progression of cancers, including ampullary carcinoma[43], biliary tract cancer[44] and neuroendocrine carcinoma[45]. In recent years, phase separation has made some breakthroughs in the field of life science and has been proven to play a key role in gene transcription. It was reported that the CRC components HOXB8 and FOSL1 formed phase-separated condensates at super-enhancers to regulate gene transcription in osteosarcoma[46]. We speculate that our CRC may upregulate EHF by phase separation formation of CRC constituents, ELF3, KLF5 and GATA6. This hypothesis needs to be verified in future studies.

TFs not only refine CRC through their interactions with other TFs and their SEs but also form complexes with cofactors to mediate transcriptional regulation[47]. In this study, we first found and verified that cofactor AJUBA interacted with EHF. Shuttling between the cytoplasm and nucleus, the LIM domain-containing protein AJUBA interacts with various proteins in the cytoplasm and nucleus, including TFs, to form various complexes[48]. On the one hand, AJUBA functions as a corepressor of snail/slug[49,50] and nuclear receptor[51] activity to weaken the transcription of their target genes. On the other hand, AJUBA serves as a coactivator that enhances the transcriptional activities of ERα[52], Aurora-A[53] and Rac[54]. In summary, AJUBA is a transcriptional corepressor or coactivator of TFs. Our study revealed, for the first time, that AJUBA functions as a coactivator of the TF EHF to cooperatively orchestrate a transcriptional network in GEA cells.

Tumorigenic activation of KRAS plays a leading role in the initiation, growth, progression, metastasis, drug resistance and recurrence of cancers[55,56]. Although many studies have been performed to identify the central roles played by KRAS mutations in cancers[57−59], less research has directly focused on the role of the KRAS protein or signaling pathway. Direct targeting of the KRAS protein has been thought impossible due to the absence of pockets for drug binding in the KRAS protein[60]. Hence, targeting a protein upstream or downstream of KRAS has been an alternative way to inhibit tumorigenic signaling. Potential drugs directly or indirectly targeting KRAS signaling have entered into preclinical or clinical trials. For example, deltarasin impaired oncogenic KRAS signaling by inhibiting the KRAS−PDEδ interaction[61]. To date, no study on the regulation of the KRAS pathway by EHF or AJUBA has been reported. Our integrative analysis involving both RNA-seq and ChIP-seq identified KRAS signaling as a key signaling pathway downstream of EHF and AJUBA, which was validated by qRT-PCR and immunoblotting.

The research focus shifted from directly targeting the KRAS protein to targeting molecules upstream or downstream of KRAS. Notably, we identified EHF and AJUBA as proteins upstream of the KRAS pathway. Targeting EHF and AJUBA can directly inhibit oncogenic KRAS signaling. However, targeting TFs with small molecules is thought to be difficult, except with the nuclear receptor family[29]. The overwhelming success of COVID-19 vaccines delivered through NPs has greatly increased public trust and universally influenced the applications of nanotechnology[62−65]. Indeed, numerous drugs based on lipid NPs have been approved for disease prevention and therapy[66−68]. Lipid NPs can provisionally compromise the permeability barrier and allow nucleic acids to enter cells[69]. In this study, we employed lipid-based NPs to deliver siRNAs against EHF and AJUBA into cancer cells and found that anchoring EHF and AJUBA through lipid-based NPs cooperatively facilitated GEA remission in cell lines and PDX models. Our results suggested that targeting EHF and AJUBA with lipid nanoparticles is an attractive potential treatment for fatal GEA.

5. Conclusions

In conclusion, EHF phenotypically facilitates the malignant biological behavior of GEA cells, and it is upregulated in GEA samples. Mechanistically, EHF is upregulated by the ELF3-KLF5-GATA6 CRC in GEA. We found for the first time that EHF interacts with cofactor AJUBA to cooperatively orchestrate a transcriptional network. Furthermore, we identified KRAS signaling as a common downstream pathway of EHF and AJUBA. In application, targeting EHF and AJUBA using lipid nanoparticles cooperatively attenuated the malignant behavior of GEA *in vitro* and *in vivo*, providing a promising novel therapeutic strategy.

Author contributions

Conceptualization and design, Li Peng, Dong Yin, Xianzhu Yang and Xiaoqing Yuan; acquisition of data, Li Peng and Xiaoqing Yuan; analysis and interpretation of data, Li Peng and Xiaoqing Yuan; drafting of the manuscript, Li Peng and Xiaoqing Yuan; critical revision of the manuscript for important intellectual content, Yanyi Jiang, Daning Lu, Xianzhu Yang, Xiaoqing Yuan and Dong Yin; statistical analysis, Li Peng and Xiaoqing Yuan; obtained funding, Li Peng, Dong Yin and Xiaoqing Yuan; administrative, technical, or material support, Li Peng, Hengxing Chen, Yongqiang Wang, Qiusheng Lan, Shuiqin Chen, Zhanwang Huang, Jingyuan Zhang, Duanqing Tian, Yuntan Qiu, Diankui Cai, Jiangyun Peng and Xianzhu Yang; study supervision, Dong Yin, Xiaoqing Yuan and Xianzhu Yang. All authors have read and agreed to the published version of the manuscript.

Conflict of interest

The authors declare that there are no relevant or material financial interests that relate to the research described in this paper.

Appendix A.   Supporting information

Supporting information to this article can be found online at https://doi.org/10.1016/j.apsb.2024.02.025.

References

1. Sung H, Ferlay J, Siegel RL, Laversanne M, Soerjomataram I, Jemal A, et al. Global cancer statistics 2020: GLOBOCAN estimates of incidence and mortality worldwide for 36 cancers in 185 countries. *CA Cancer J Clin* 2021;**71**:209−49.
2. Smyth EC, Nilsson M, Grabsch HI, van Grieken NC, Lordick F. Gastric cancer. *Lancet* 2020;**396**:635−48.
3. Ajani JA, Lee J, Sano T, Janjigian YY, Fan D, Song S. Gastric adenocarcinoma. *Nat Rev Dis Primers* 2017;**3**:17036.
4. Integrated genomic characterization of oesophageal carcinoma. *Nature* 2017;**541**:169−75.
5. Joshi SS, Badgwell BD. Current treatment and recent progress in gastric cancer. *CA Cancer J Clin* 2021;**71**:264−79.
6. Hofheinz RD, Haag GM, Ettrich TJ, Borchert K, Kretzschmar A, Teschendorf C, et al. Perioperative trastuzumab and pertuzumab in combination with FLOT versus FLOT alone for HER2-positive resectable esophagogastric adenocarcinoma: final results of the PETRARCA multicenter randomized phase II trial of the AIO. *J Clin Oncol* 2020;**38**:4502.
7. Al-Batran SE, Hofheinz RD, Schmalenberg H, Strumberg D, Goekkurt E, Angermeier S, et al. Perioperative ramucirumab in combination with FLOT versus FLOT alone for resectable esophagogastric adenocarcinoma (RAMSES/FLOT7): results of the phase II-portion—a multicenter, randomized phase II/III trial of the German AIO and Italian GOIM. *J Clin Oncol* 2020;**38**:4501.
8. Yoshida K, Kodera Y, Kochi M, Ichikawa W, Kakeji Y, Sano T, et al. Addition of docetaxel to oral fluoropyrimidine improves efficacy in patients with stage III gastric cancer: interim analysis of JACCRO GC-07, a randomized controlled trial. *J Clin Oncol* 2019;**37**:1296−304.
9. Nagaraja AK, Kikuchi O, Bass AJ. Genomics and targeted therapies in gastroesophageal adenocarcinoma. *Cancer Discov* 2019;**9**:1656−72.
10. Bradner JE, Hnisz D, Young RA. Transcriptional addiction in cancer. *Cell* 2017;**168**:629−43.
11. Shi X, Zheng Y, Jiang L, Zhou B, Yang W, Li L, et al. EWS-FLI1 regulates and cooperates with core regulatory circuitry in Ewing sarcoma. *Nucleic Acids Res* 2020;**48**:11434−51.
12. Henley MJ, Koehler AN. Advances in targeting 'undruggable' transcription factors with small molecules. *Nat Rev Drug Discov* 2021;**20**:669−88.
13. Bushweller JH. Targeting transcription factors in cancer—from undruggable to reality. *Nat Rev Cancer* 2019;**19**:611−24.
14. Ma S, Zhou B, Yang Q, Pan Y, Yang W, Freedland SJ, et al. A Transcriptional regulatory loop of master regulator transcription factors, PPARG, and fatty acid synthesis promotes esophageal adenocarcinoma. *Cancer Res* 2021;**81**:1216−29.
15. Chen L, Huang M, Plummer J, Pan J, Jiang YY, Yang Q, et al. Master transcription factors form interconnected circuitry and orchestrate transcriptional networks in oesophageal adenocarcinoma. *Gut* 2020;**69**:630−40.
16. Wang L, Ai M, Nie M, Zhao L, Deng G, Hu S, et al. EHF promotes colorectal carcinoma progression by activating TGF-β1 transcription and canonical TGF-β signaling. *Cancer Sci* 2020;**111**:2310−24.
17. Wu J, Duan R, Cao H, Field D, Newnham CM, Koehler DR, et al. Regulation of epithelium-specific Ets-like factors ESE-1 and ESE-3 in airway epithelial cells: potential roles in airway inflammation. *Cell Res* 2008;**18**:649−63.
18. Zhu P, Wu J, Wang Y, Zhu X, Lu T, Liu B, et al. LncGata6 maintains stemness of intestinal stem cells and promotes intestinal tumorigenesis. *Nat Cell Biol* 2018;**20**:1134−44.
19. Duffy MJ, O'Grady S, Tang M, Crown J. MYC as a target for cancer treatment. *Cancer Treat Rev* 2021;**94**:102154.
20. Chen H, Pugh BF. What do transcription factors interact with?. *J Mol Biol* 2021;**433**:166883.
21. Peng L, Jiang B, Yuan X, Qiu Y, Peng J, Huang Y, et al. Super-enhancer-associated long noncoding RNA HCCL5 is activated by ZEB1 and promotes the malignancy of hepatocellular carcinoma. *Cancer Res* 2019;**79**:572−84.
22. Peng JY, Cai DK, Zeng RL, Zhang CY, Li GC, Chen SF, et al. Upregulation of superenhancer-driven lncRNA FASRL by USF1 promotes de novo fatty acid biosynthesis to exacerbate hepatocellular carcinoma. *Adv Sci (Weinh)* 2023;**10**:e2204711.
23. Yuan XQ, Zhou N, Wang JP, Yang XZ, Wang S, Zhang CY, et al. Anchoring super-enhancer-driven oncogenic lncRNAs for anti-tumor therapy in hepatocellular carcinoma. *Mol Ther* 2023;**31**:1756−74.
24. Camp RL, Dolled-Filhart M, Rimm DL. X-tile: a new bio-informatics tool for biomarker assessment and outcome-based cut-point optimization. *Clin Cancer Res* 2004;**10**:7252−9.

25. Lambert SA, Jolma A, Campitelli LF, Das PK, Yin Y, Albu M, et al. The human transcription factors. *Cell* 2018;**172**:650−65.

26. Wang Z, Wang P, Li Y, Peng H, Zhu Y, Mohandas N, et al. Interplay between cofactors and transcription factors in hematopoiesis and hematological malignancies. *Signal Transduct Target Ther* 2021;**6**:24.

27. Jiang Y, Jiang YY, Lin DC. Super-enhancer-mediated core regulatory circuitry in human cancer. *Comput Struct Biotechnol J* 2021;**19**:2790−5.

28. Haberle V, Stark A. Eukaryotic core promoters and the functional basis of transcription initiation. *Nat Rev Mol Cell Biol* 2018;**19**: 621−37.

29. Overington JP, Al-Lazikani B, Hopkins AL. How many drug targets are there?. *Nat Rev Drug Discov* 2006;**5**:993−6.

30. Taiariol L, Chaix C, Farre C, Moreau E. Click and bioorthogonal chemistry: the future of active targeting of nanoparticles for nano-medicines?. *Chem Rev* 2022;**122**:340−84.

31. Wang C, Zhang Y, Dong Y. Lipid Nanoparticle-mRNA formulations for therapeutic applications. *Acc Chem Res* 2021;**54**:4283−93.

32. Li W, Qiu J, Li XL, Aday S, Zhang J, Conley G, et al. BBB pathophysiology-independent delivery of siRNA in traumatic brain injury. *Sci Adv* 2021;**7**:eabd6889.

33. Zhang T, Song X, Zhang Z, Mao Q, Xia W, Xu L, et al. Aberrant super-enhancer landscape reveals core transcriptional regulatory circuitry in lung adenocarcinoma. *Oncogenesis* 2020;**9**:92.

34. Shi J, Qu Y, Li X, Sui F, Yao D, Yang Q, et al. Increased expression of EHF *via* gene amplification contributes to the activation of HER family signaling and associates with poor survival in gastric cancer. *Cell Death Dis* 2016;**7**:e2442.

35. Zhao T, Jiang W, Wang X, Wang H, Zheng C, Li Y, et al. ESE3 in-hibits pancreatic cancer metastasis by upregulating E-cadherin. *Cancer Res* 2017;**77**:874−85.

36. Zhou T, Liu J, Xie Y, Yuan S, Guo Y, Bai W, et al. ESE3/EHF, a promising target of rosiglitazone, suppresses pancreatic cancer stem-ness by downregulating CXCR4. *Gut* 2022;**71**:357−71.

37. Sakamoto K, Endo K, Sakamoto K, Kayamori K, Ehata S, Ichikawa J, et al. EHF suppresses cancer progression by inhibiting ETS1-mediated ZEB expression. *Oncogenesis* 2021;**10**:26.

38. Huang WC, Jang TH, Tung SL, Yen TC, Chan SH, Wang LH. A novel miR-365-3p/EHF/keratin 16 axis promotes oral squamous cell carci-noma metastasis, cancer stemness and drug resistance *via* enhancing β5-integrin/c-met signaling pathway. *J Exp Clin Cancer Res* 2019;**38**:89.

39. Li M, Huang H, Li L, He C, Zhu L, Guo H, et al. Core transcription regulatory circuitry orchestrates corneal epithelial homeostasis. *Nat Commun* 2021;**12**:420.

40. Durbin AD, Zimmerman MW, Dharia NV, Abraham BJ, Iniguez AB, Weichert-Leahey N, et al. Selective gene dependencies in MYCN-amplified neuroblastoma include the core transcriptional regulatory circuitry. *Nat Genet* 2018;**50**:1240−6.

41. Jiang YY, Jiang Y, Li CQ, Zhang Y, Dakle P, Kaur H, et al. TP63, SOX2, and KLF5 establish a core regulatory circuitry that controls epigenetic and transcription patterns in esophageal squamous cell carcinoma cell lines. *Gastroenterology* 2020;**159**:1311−1327.e19.

42. Rubin AJ, Barajas BC, Furlan-Magaril M, Lopez-Pajares V, Mumbach MR, Howard I, et al. Lineage-specific dynamic and pre-established enhancer-promoter contacts cooperate in terminal differ-entiation. *Nat Genet* 2017;**49**:1522−8.

43. Yachida S, Wood LD, Suzuki M, Takai E, Totoki Y, Kato M, et al. Genomic sequencing identifies ELF3 as a driver of ampullary carci-noma. *Cancer Cell* 2016;**29**:229−40.

44. Suzuki M, Saito-Adachi M, Arai Y, Fujiwara Y, Takai E, Shibata S, et al. E74-like factor 3 is a key regulator of epithelial integrity and immune response genes in biliary tract cancer. *Cancer Res* 2021;**81**: 489−500.

45. Horie M, Tanaka H, Suzuki M, Sato Y, Takata S, Takai E, et al. An integrative epigenomic approach identifies ELF3 as an oncogenic

46. regulator in ASCL1-positive neuroendocrine carcinoma. *Cancer Sci* 2023;**114**:2596−608.

46. Lu B, Zou C, Yang M, He Y, He J, Zhang C, et al. Pharmacological inhibition of core regulatory circuitry liquid−liquid phase separation suppresses metastasis and chemoresistance in osteosarcoma. *Adv Sci (Weinh)* 2021;**8**:e2101895.

47. Wang Y, Viscarra J, Kim SJ, Sul HS. Transcriptional regulation of hepatic lipogenesis. *Nat Rev Mol Cell Biol* 2015;**16**:678−89.

48. Jia H, Peng H, Hou Z. Ajuba: an emerging signal transducer in oncogenesis. *Pharmacol Res* 2020;**151**:104546.

49. Langer EM, Feng Y, Zhaoyuan H, Rauscher 3rd FJ, Kroll KL, Longmore GD. Ajuba LIM proteins are snail/slug corepressors required for neural crest development in Xenopus. *Dev Cell* 2008;**14**: 424−36.

50. Ayyanathan K, Peng H, Hou Z, Fredericks WJ, Goyal RK, Langer EM, et al. The Ajuba LIM domain protein is a corepressor for SNAG domain mediated repression and participates in nucleocyto-plasmic shuttling. *Cancer Res* 2007;**67**:9097−106.

51. Hou Z, Peng H, White DE, Negorev DG, Maul GG, Feng Y, et al. LIM protein Ajuba functions as a nuclear receptor corepressor and nega-tively regulates retinoic acid signaling. *Proc Natl Acad Sci U S A* 2010;**107**:2938−43.

52. Xu B, Li Q, Chen N, Zhu C, Meng Q, Ayyanathan K, et al. The LIM protein Ajuba recruits DBC1 and CBP/p300 to acetylate ERα and enhances ERα target gene expression in breast cancer cells. *Nucleic Acids Res* 2019;**47**:2322−35.

53. Hirota T, Kunitoku N, Sasayama T, Marumoto T, Zhang D, Nitta M, et al. Aurora-A and an interacting activator, the LIM protein Ajuba, are required for mitotic commitment in human cells. *Cell* 2003;**114**: 585−98.

54. Nola S, Daigaku R, Smolarczyk K, Carstens M, Martin-Martin B, Longmore G, et al. Ajuba is required for Rac activation and mainte-nance of E-cadherin adhesion. *J Cell Biol* 2011;**195**:855−71.

55. Yang Z, Xu G, Wang B, Liu Y, Zhang L, Jing T, et al. USP12 downregulation orchestrates a protumourigenic microenvironment and enhances lung tumour resistance to PD-1 blockade. *Nat Commun* 2021;**12**:4852.

56. Buscail L, Bournet B, Cordelier P. Role of oncogenic KRAS in the diagnosis, prognosis and treatment of pancreatic cancer. *Nat Rev Gastroenterol Hepatol* 2020;**17**:153−68.

57. Lundy J, Gao H, Berry W, Masoumi-Moghoddam S, Jenkins BJ, Croagh D. Targeted transcriptome and KRAS mutation analysis improve the diagnostic performance of EUS-FNA biopsies in pancreatic cancer. *Clin Cancer Res* 2021;**27**:5900−11.

58. Finn SP, Addeo A, Dafni U, Thunnissen E, Bubendorf L, Madsen LB, et al. Prognostic impact of KRAS G12C mutation in patients with NSCLC: results from the European Thoracic Oncology Platform Lungscape project. *J Thorac Oncol* 2021;**16**:990−1002.

59. Liu Z, Liu Y, Qian L, Jiang S, Gai X, Ye S, et al. A proteomic and phosphoproteomic landscape of KRAS mutant cancers identifies combination therapies. *Mol Cell* 2021;**81**:4076−4090.e8.

60. Chen K, Zhang Y, Qian L, Wang P. Emerging strategies to target RAS signaling in human cancer therapy. *J Hematol Oncol* 2021;**14**: 116.

61. Zimmermann G, Papke B, Ismail S, Vartak N, Chandra A, Hoffmann M, et al. Small molecule inhibition of the KRAS−PDEδ interaction impairs oncogenic KRAS signalling. *Nature* 2013;**497**: 638−42.

62. Khurana A, Allawadhi P, Khurana I, Allwadhi S, Weiskirchen R, Banothu AK, et al. Role of nanotechnology behind the success of mRNA vaccines for COVID-19. *Nano Today* 2021;**38**:101142.

63. Elia U, Ramishetti S, Rosenfeld R, Dammes N, Bar-Haim E, Naidu GS, et al. Design of SARS-CoV-2 hFc-conjugated receptor-binding domain mRNA vaccine delivered *via* lipid nanoparticles. *ACS Nano* 2021;**15**:9627−37.

64. Tenchov R, Bird R, Curtze AE, Zhou Q. Lipid nanoparticles-from liposomes to mRNA vaccine delivery, a landscape of research diversity and advancement. *ACS Nano* 2021;**15**:16982−7015.

65. Zhang Y, Sun C, Wang C, Jankovic KE, Dong Y. Lipids and lipid derivatives for RNA delivery. *Chem Rev* 2021;**121**:12181−277.

66. Adams D, Gonzalez-Duarte A, O'Riordan WD, Yang CC, Ueda M, Kristen AV, et al. Patisiran, an RNAi therapeutic, for hereditary transthyretin amyloidosis. *N Engl J Med* 2018;**379**:11−21.

67. Miao L, Zhang Y, Huang L. mRNA vaccine for cancer immunotherapy. *Mol Cancer* 2021;**20**:41.

68. Wang D, Sun Y, Liu Y, Meng F, Lee RJ. Clinical translation of immunoliposomes for cancer therapy: recent perspectives. *Expert Opin Drug Deliv* 2018;**15**:893−903.

69. Kulkarni JA, Witzigmann D, Thomson SB, Chen S, Leavitt BR, Cullis PR, et al. The current landscape of nucleic acid therapeutics. *Nat Nanotechnol* 2021;**16**:630−43.